Turkish Journal of Electrical Engineering and Computer Sciences

Volume 6 | Number 3 Article 1

1-1-1998

State of Art in Realistic Head Modeling for Electro-magnetic Source Imaging of the Human Brain

NEVZAT G. GENÇER

İ. OĞUZ TANZER

M. KEMAL ÖZDEMİR

CAN E. ACAR

MERT SUNGUR

ELEKTRİK, VOL.6, NO.3, 1998, ©TÜBİTAK

State of Art in Realistic Head Modeling for Electro-magnetic Source Imaging of the Human Brain*

Nevzat G. Gençer*, I. Oğuz Tanzer, M. Kemal Özdemir,
Can E. Acar and Mert Sungur
Department of Electrical and Electronics Engineering
Middle East Technical University, 06531 Balgat, Ankara, TURKEY
E-mail: ngencer@ed.eee.metu.edu.tr

Abstract

Electric currents produced by the neural activity in the brain create electric potentials on the scalp and magnetic field distribution outside the scalp. Measuring electric and magnetic fields provides a means to understand the spatio-temporal distribution of the neural activity. The representations of the intracellular electric current of active cell populations based on bimodal data are called electro-magnetic source image (EMSI). With the recent development of large arrays of magnetic sensors, and systems for measuring scalp voltages at more than 100 locations, it is now feasible to implement computational methods that employ numerical models which incorporate the correct geometry and electrical properties of the head. This paper introduces the problem of developing realistic head models for generating more accurate EMSIs. In that sense it has a major review component. Tissue classification from magnetic resonance images forms the first step for realistic head modeling. Thus existing segmentation algorithms and their performances will be discussed. Next, two numerical methods, namely the Finite Element Method (FEM) and the Boundary Element Method (BEM), will be introduced for the solution of electric potential and magnetic fields for a known source configuration. An overall measure, relative difference measure (RDM) is used to measure the performance of the numerical models implemented using isoparametric, quadratic elements. It is observed that both FEM and BEM models yield RDMs around 1%. Finally, a methodology is introduced for parallel implementation of FEM. The implemented parallelization algorithm provided a speed-up of 1.49 on two processors, for a 31769 noded mesh.

1. Introduction

Advances in technology during the past few decades provided a number of modalities to explore the functional organization of the human brain. Historically, the positron emission tomography (PET) was the first to measure brain functions quantitatively. PET reveals where the administered positron-emitting nuclei become concentrated in the body [1], for instance as a tag on a neurotransmitter. However, the response time for PET may be as long as several seconds. More recently, a new technique named functional magnetic resonance imaging (fMRI) has provided a means to monitor the local changes in blood flow rate or blood volume [2]-[6]. In these methods, however, the subject is exposed to either radioactive tracers or to time-varying and strong

* This work is supported by Turkish Scientific and Technical Research Council Project EEEAG-192

magnetic fields. In the electrical techniques that use electric and magnetic field measurements, on the other hand, no energy is applied to the subject. Thus, the electrical methods are completely noninvasive.

Electric potential and magnetic fields associated with the intracellular currents that flow within the active pyramidal cells of the cortex provide a means to monitor the spatio-temporal evolution of the cortical activity within the human brain. Recording electrical potential differences from the scalp surface (electroencephalography) is possible via surface electrodes. The weak magnetic fields outside the head surface can be obtained by superconducting quantum interference device (SQUID) magnetometer (magnetoencephalography) [7, 8]. Thus by measuring potentials and magnetic fields, it is possible to demonstrate continuous brain activity. Moreover, one goal in electric and magnetic recordings is to form an image of the electrical sources distributed across the cortex. Such representations, obtained via event related measurements, provide a noninvasive means to obtain information about the centers of related brain functions. For convenience, we call such a representation *electric source image* (ESI) when it is based on electric data, *magnetic source image* (MSI) when the images are obtained via magnetic data, and *electromagnetic source image* (EMSI) when it is based on bimodal data.

The electric potential patterns on the scalp surface and the magnetic field patterns measured near the head are similar to the field patterns of a dipole source (Fig. 1). As a result, the *current dipole model* is traditionally employed to represent the center of simultaneously active neural sources. Finding a representation for the source distribution corresponds to finding the locations and directions of the current dipoles from the measurement patterns at consecutive instants. Several methods have been suggested to solve this problem which is referred to as the *inverse problem*. Multiple dipole fits are developed to find the directions and locations of a number of dipoles [10]-[13]. Such methods are non-linear as the dipole locations are non-linearly related to the measurements. If the dipole locations are obtained by some means then it is possible to apply linear inversion methods, as the measurements are linearly dependent to the dipole strengths. Physiological studies reveal that the pyramidal cells are normal to the cortical surface, imposing currents to flow parallel to the surface normal at that point (Fig. 2). Thus it is possible to make use of linear methods by applying the following three steps: 1) obtain the cortical surface by applying segmentation algorithms to the MRI data, 2) define a grid on the cortical surface (each pixel represents a neural population confined to a small area which are directed parallel to the surface normal) 3) calculate the potential difference or magnetic field for each unit dipole on that grid (this forms the entries of the coefficient matrix relating the measurements to the dipole strengths). The locations and directions of finite number of dipoles (typically ten thousands) are then known but their strengths are unknowns.

Linear and non-linear methods in numerical computations are based on differences between measurements and calculated fields obtained for an estimated source configuration. Thus solution of potential and/or magnetic fields for a given dipole configuration (*forward problem*) is required. In previous studies, the forward problem was usually solved for simple models of the head. However, the accuracy in dipole solutions is highly affected by the discrepancy between the head model used and the actual head [10, 11, 13]. If a realistic head model is to be used, complicated numerical methods have to be applied to solve these fields accurately.

In order to obtain accurate representations of pysiological sources, the associated fields must be properly sampled. The recent advent of very large arrays of electrodes and superconducting sensors provide magnetoencephalography (MEG) and electroencephalography (EEG) data from over two hundred channels. In addition to the need for sufficent number of data, a methodology must be developed to accurately model the subject's head. New generation magnetic resonance imaging (MRI) systems provide images with spatial resolution under 1 mm. The progress in computer technology continuously increases the speed and memory

capabilities of even personal computers. Thus it is now an appropriate time to launch an effort on the development of accurate head models of individuals. This will incorporate the correct geometry of the head and electrical properties of the tissues, thus yielding a better interpretation of the measured data.

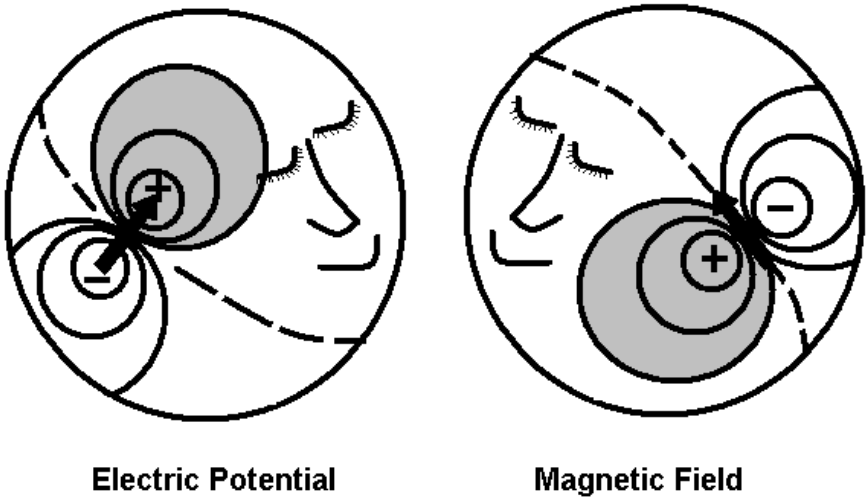

Figure 1. Field patterns for a current dipole in spherical conductive body.

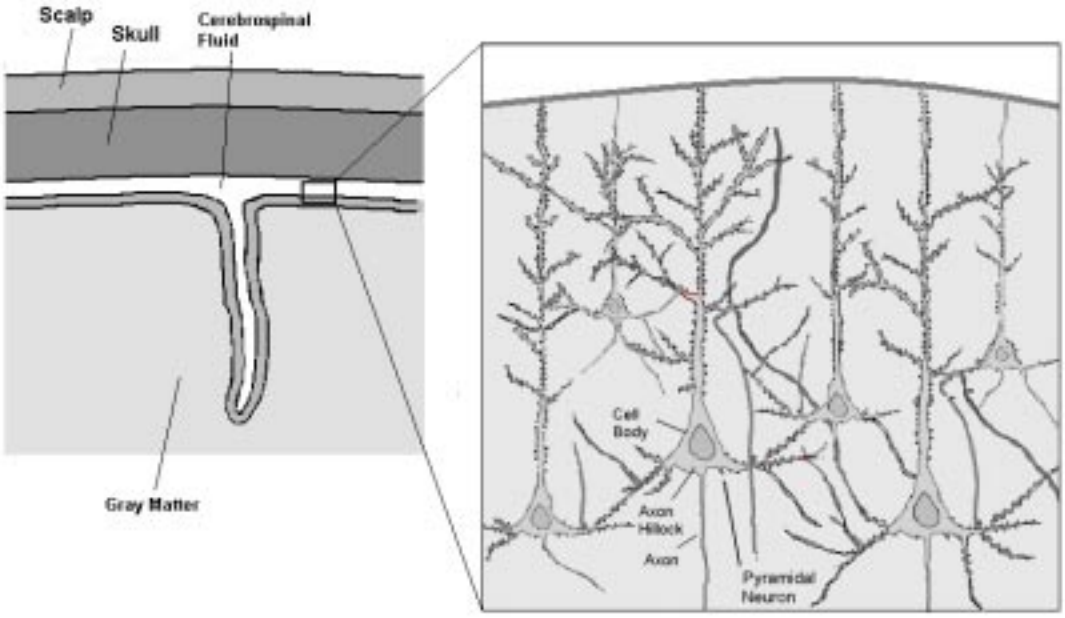

Figure 2. An illustration of the location of pyramidal neurons relative to the cortex surface. The orientation of the neurons are such that they are normal to the cortex surface

In this study, first different approaches will be presented for the solution of the tissue classification problem. Next, the two numerical methods, namely, FEM and BEM will be introduced to solve the electric and magnetic fields. Comparative results will be given for single dipole sources at different depths. A methodology for parallel implementation of the FEM will be presented and preliminary results will be provided.

2. Tissue Classification from MRI Data

The objective is to obtain a numerical model of the human head based on the geometry information and the electrical properties of the classified tissues. In this study, we will introduce the problem of tissue classification as the basis of realistic head modeling for electro-magnetic source imaging.

The tissue classification process consists of three sub-operations: segmentation, labeling and surface parametrization. Segmentation provides a discrete 3-D set of data that belongs to a specific tissue and labeling identifies the tissue type (Figure 3). Finally, a surface reconstruction algorithm provides a list of polygons to represent the convoluted surface of the tissue for visualization purposes (Figure 4).

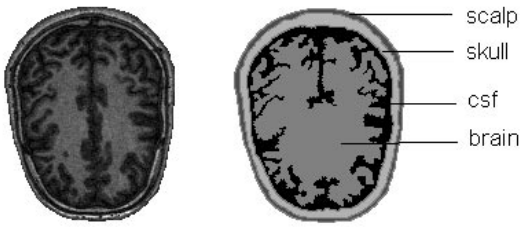

Figure 3. A sample MR slice and the corresponding segmented MR slice

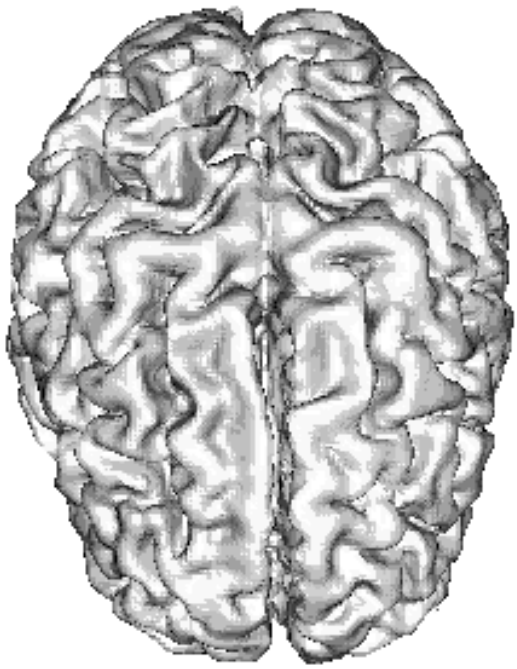

Figure 4. A sample brain surface extracted from 3D MR data

In general, segmentation algorithms are applied to a number of two-dimensional (2-D) MRI data. One way of doing this is to allow an expert to decide and record which pixel belongs to which tissue. Obviously, such manual segmentation procedures are tedious and time-consuming. On the other hand, automatic

segmentation of MR brain images by means of a computer without human intervention is a difficult task. The difficulty lies in the complexity of the structures to be detected, the intrascan and interscan intensity inhomogeneities in the MR images, variable imaging conditions, noise, the partial volume effect where one voxel contains more than one type of tissue, and the anatomical variations in brain structures. This task basically requires the integration of complicated image processing with high-level information about the structures to be segmented. Below, the approaches toward the fully automatic segmentation of MR brain images are summarized.

Classical low-level image segmentation techniques include similarity- and boundary-based methods [15]. Image segmentation approaches like region growing and split-and-merge methods are based on the similarities of voxel intensities. Thus, they are dependent on the choice of similarity criteria and may not provide satisfactory results if used alone in MR images. In boundary-based segmentation methods, edges in the images are detected and then linked to extract boundaries of structures. These methods are also difficult to apply to complex medical images. Similarity- or boundary-based methods can be improved to provide more reliable results by taking into account apriori knowledge about the structures to be segmented and by using the 3D information obtained from neighbouring MR slices [16, 17, 18].

Another approach in the segmentation of MR images is to cluster the image into classes by pattern recognition methods. Classical Bayes classifiers, supervised and unsupervised artificial neural networks, fuzzy models and fuzzy neural networks are commonly used models for this purpose [19, 20]. These techniques are quite sensitive to the choice of initial values for the model parameters and to the selection of training data. Unsupervised techniques provide better performance with less human intervention but they are slow.

Some more advanced techniques are based on the concept of deformable models. Active contours [25] in two dimensions and their three-dimensional extension, active surfaces [21, 26], combine the boundary-based techniques with the use of high-level information about the structures to be segmented. In these techniques, the contour or the surface is deformed so as to minimize its total energy under the influence of internal and external forces.

Given a contour v as a mapping $[0,1] \rightarrow \Re^2$ and its energy on any point s on the contour

$$E(v(s)) = E_{internal} + E_{external} \tag{1}$$

the contour is deformed in such a way to minimize its total energy

$$E(v) = \int_0^1 E(v(s))ds \tag{2}$$

The external image-based forces such as the edge force are responsible for the boundary detection, whereas the internal forces determine the shape and curvature constraints. The internal energy is generally given by

$$E_{internal}(s) = \alpha(s)l\frac{dv}{ds}\|^2 + \beta(s)\|\frac{d^2v}{ds^2}\|^2 \tag{3}$$

where the first term provides elasticity and the second term provides rigidity (α and β are the respective weight functions along the contour). The external energy is chosen such that the contour will be attracted by the desired image features. For example, given the image I, an energy term such as

$$E_{edge} = -\|\nabla I\|^2 \tag{4}$$

will attract the contour towards the local maxima of the gradient, i.e the edges.

Similar to active contours, an active surface is described by a mapping $[0,1] \times [0,1] \rightarrow \Re^3$ and the total energy of the surface is given by

$$E(v) = \int_0^1 \int_0^1 E(v(s,r))dsdr \tag{5}$$

Proper initialization of the contour or the surface, the selection of the elasticity parameters in the internal energy expression and energy minimization are the basic problems encountered in the deformable models. Studies in this field are focused on developing efficient techniques for energy minimization and proposing new active contour and surface models for better segmentation of complex structures [21, 22, 23, 24, 27, 28, 29]. A closely related approach is to deform a standard brain atlas using image warping so as to fit the MR image in hand, thus labeling the structures in the image by matching with the labels of the atlas [30, 31]. Once the tissue classification is complete, the resulting geometrical model, together with the assigned electrical properties of the tissues will be used to obtain numerical solutions.

3. Numerical Methods for the Forward Problem

Current dipoles have been assumed to be adequate to represent the electrical sources in the human brain [9]. Thus, the forward problem in electro-magnetic source imaging is defined as finding the electric potential pattern on the scalp surface and the magnetic field pattern just outside the scalp for a given dipole distribution. In this section, the governing partial differential equations for the electric potential and the magnetic field density will be presented first. Next, analytical solutions will be provided which are available for simple source configurations and body geometries. Finally, two numerical solution methods, namely, the Finite Element Method and the Boundary Element Method, will be discussed for the solution of the associated fields for objects of arbitrary geometry and conductivity distributions.

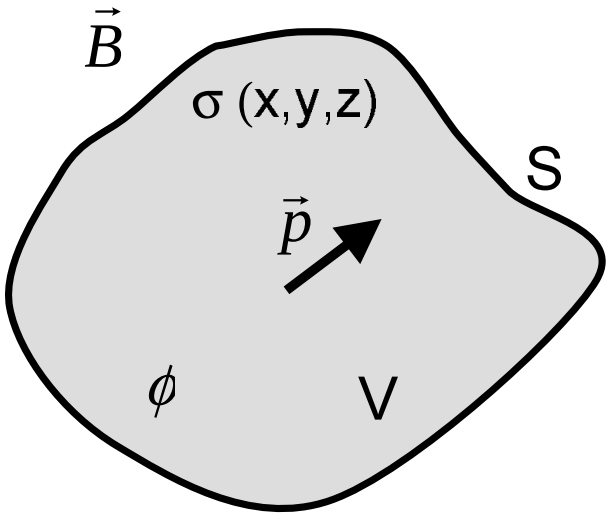

Figure 5. A current dipole $\vec{p}$ in an inhomogeneous conductive body of volume V and surface S. The current dipole is defined by the primary current density $\vec{J}^p$ in a differential volume element dv ($\vec{p} = \vec{J}^p dv$). The conductivity distribution is denoted by σ. Φ represents the potential distribution in volume V and surface S while $\vec{B}$ is the magnetic field density near the conductive body.

Fig. 5 shows a current dipole $\vec{p}$ in a body of inhomogeneous conductivity. The potential distribution Φ and magnetic field distribution $\vec{B}$ due to primary currents $\vec{J^p}$ satisfy the following partial differential equations.

$$\begin{aligned} \nabla \cdot \sigma \nabla \Phi &= -\nabla \cdot \vec{J^p} \quad in \quad V \qquad (6) \\ \sigma \frac{\partial \Phi}{\partial n} &= 0 \quad on \quad S \qquad (7) \end{aligned}$$

and

$$\begin{aligned} \nabla^2 \vec{B} &= -\mu_0 \nabla \times \vec{J} \\ \vec{B} &= 0 \quad at \quad \infty \qquad (8) \end{aligned}$$

where V is volume and S is the surface of the body. Here $\vec{J}$ is defined as $\vec{J} = \vec{J^p} - \sigma \nabla \Phi$. The two equations given above are of Poisson's type and have analytical solutions when the body geometry and conductivity distribution are simple. For example, for an unbounded uniform medium, the potential and magnetic field distributions can be represented as;

$$\Phi(r) = \frac{1}{4\pi\sigma} \frac{\vec{p} \cdot \vec{R}}{R^3} \qquad (9)$$

$$\vec{B}(r) = \frac{\mu_0}{4\pi} \frac{\vec{p} \times \vec{R}}{R^3} \qquad (10)$$

where $\vec{R}$ is the vector from the source point to the field point. When the source is located in the center of a spherical homogeneous body the field solutions are

$$\begin{aligned} \Phi(r) &= \frac{3}{4\pi\sigma} \frac{\vec{p} \cdot \vec{R}}{R^3} \\ \vec{B}(r) &= 0 \qquad (11) \end{aligned}$$

Another simple source body configuration is for a dipole shifted b units from the center of a sphere with radius R_s. The corresponding solutions for the point (θ_p, ϕ_p) are:

$$\Phi(\theta_p, \phi_p) = \frac{p_z}{4\pi\sigma R_s^2} [\frac{1 - f^2}{(1 - 2f\mu + f^2)^{3/2}} - 1] + \frac{p_x Cos\theta_p + p_y Sin\theta_p)}{4\pi\sigma f R_s^2 Sin\theta_p} [\frac{f^3 - 3f^2\mu + 3f - \mu}{1 + f^2 - 2f\mu} + \mu] \qquad (12)$$

Here μ and f are defined as $\mu = Cos\theta_p$ and $f = b/R_s$. In that case, the magnetic field density $\vec{B}$ is obtained using the following expressions:

$$\begin{aligned} U(R, \theta, \phi) &= \frac{p_x Sin\phi}{4\pi b Sin\theta} \frac{bCos\theta - R}{\sqrt{R^2 - 2bRCos\theta + b^2}} \\ \vec{B} &= -\mu_0 \nabla U \qquad (13) \end{aligned}$$

However, for realistic head models the above analytical solutions are not applicable. For such cases numerical solutions must be employed. The Finite Element Method (FEM) and the Boundary Element Method (BEM) are two computational techniques for the forward problem solution in electro-magnetic source imaging.

3.1. Finite Element Method

FEM has been used by many investigators. Thevenet *et. al* applied the 3D FEM formulation to a three concentric sphere region [32]. Yan *et. al* computed FEM forward solutions with hexahedral elements to simulate the head with three concentric shells [33]. In a recent study, a FEM based deblurring algorithm was applied to reduce the spatial blur imposed by skull on scalp recorded brain potentials [34]. In these studies, the head models do not sufficiently represent the actual conductivity profile. However, this is essential for correct interpretation of the electric data.

In FEM, the region of interest is divided into the so-called *elements*. An equivalent discretized model is constructed for each element and then all the element contributions to the system are assembled [35]. The elements can have various shapes, such as triangles and rectangles, allowing the use of an irregular grid. Fig. 6 shows typical 3D element types, like a cubic element and an isoparametric quadratic cubic element.

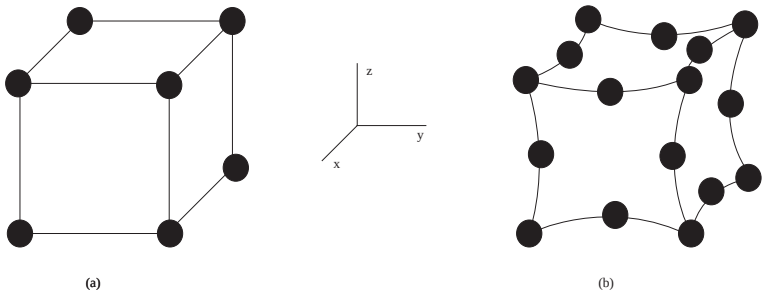

Figure 6. Different element types for 3-D FEM formulations. (a) 8-noded cubic element,(b) 20-noded hexahedral isoparametric element

The term "isoparametric" means that both variation in the geometry of the element and the potential distribution on the elements are defined with the same functions. Isoparametric elements provide two important advantages; 1) the edges of the elements can be parabolic leading to represent complicated geometries with fewer elements [35], 2) instead of using many simple elements, few complex elements can be used resulting in more accurate results. Fig. 7 shows a sphere which is subdivided into 20 noded hexahedral unit elements.

For the implementation of FEM, the conductive body is be divided into n volume elements. Using Galerkin's weighted residuals method [35], the partial differential equation for potential is satisfied across each element by multiplying both sides with an appropriate shape function and integrating throughout the element volume. For an isoparametric quadratic element, 20 shape functions are used, providing 20 linear equations for the local element node potentials. Similar equations can be derived for each element, and after an appropriate assembly of the elements that have common nodes, the following matrix equation is obtained:

$$\mathbf{A}(\sigma)\Phi = c \tag{14}$$

Here Φ is an $l \times 1$ vector representing unknown node potentials; σ denotes the $n \times 1$ vector of element conductivities; $\mathbf{A}$ is a sparse, positive definite and symmetric $l \times l$ matrix calculated by using element geometry and element conductivities, and c is the $l \times 1$ vector that incorporates the primary current density information. After choosing a reference node and making appropriate modifications in (14), it is convenient to refer to node values as voltages relative to that reference node. Since the potential distribution on the elements is the linear combination of the potentials at the node of elements, once Φ is solved, potential at

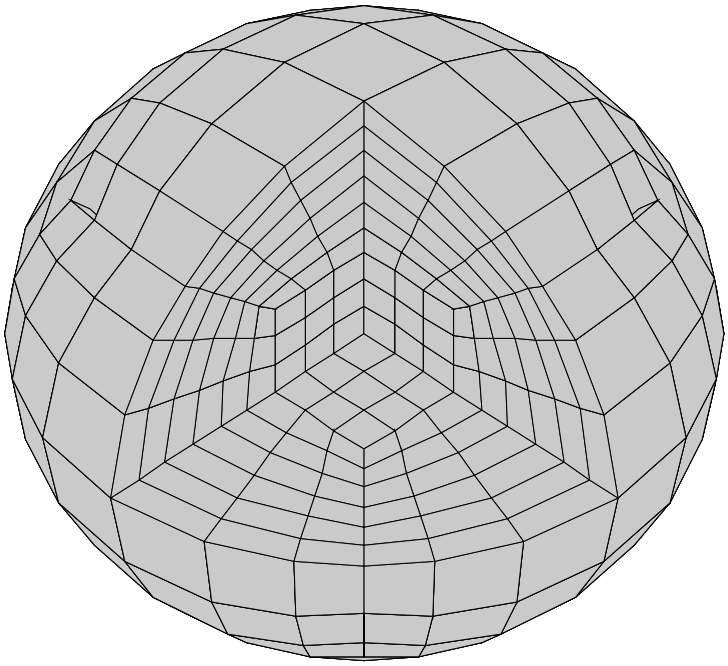

Figure 7. A typical FEM mesh for a unit sphere with 6433 nodes and 1512 elements

For a realistic head model, the finite element mesh must have a large number of elements. Thus the resulting matrix equation is too large to be solved directly on a single workstation. Instead, a network of workstations can be used as a parallel programming environment. This approach represents a trend in computing which has become popular in recent years [36]-[40]. A network of workstations called a *cluster* has many similarities to a distributed memory parallel architecture. The local area network is the message passing medium and each workstation is a processing node. A programming library such as PVM (Parallel Virtual Machine) enables programs to use this cluster as a single parallel architecture, thus combining the memory resources and processing powers of every available workstation [38]. Using this architecture, it will be possible to solve the large matrix equations using the computational resources available at most research facilities.

The finite element formulation results in a matrix equation of the form $\mathbf{A}\Phi = c$ as discussed above. In this equation $\mathbf{A}$ is a large sparse positive definite matrix. For the source localization problem, the forward problem will have to be solved for many different dipole positions. Therefore the same matrix will have to be solved for many different right-hand-side vectors. As a result, the Cholesky factorization method is preferred over iterative methods [41]. Cholesky factorization is a specialized version of Gaussian elimination for positive definite matrices. The matrix is factorized into $\mathbf{A} = \mathbf{L}\mathbf{L}^{\mathbf{T}}$ form from which the solution vector can be obtained directly. The factorization usually causes *fill-in* terms thus requiring additional storage [42].

There is a rich literature covering solution of sparse positive-definite systems, for different parallel architectures [43]-[45]. Although most of this literature covers massively parallel systems (MPPs), basic ideas can be adopted to workstation clusters. To solve a matrix equation in parallel, different parts of the matrix need to be assigned to different processors. These can be individual matrix entries, rows of the matrix or sub-blocks of the matrix depending on the algorithm used. Then, either a parallel Cholesky

factorization algorithm or a multi-frontal algorithm will be used to perform the factorization. The aim is to reduce inter-processor communications, and to utilize every processor as efficiently as possible.

The parallel architecture used in this study is a cluster of workstations. A workstation cluster usually has a small number of processors and slow communications links compared to a massively parallel computer. Therefore, the workstation cluster it is not suitable for fine-grained parallelism. The approach taken is to partition the coefficient matrix into blocks using a graph partitioning algorithm [46] and using the *asymmetric factorization* algorithm [42] over the partitioned matrix. The blocks are created by partitioning the elements in the finite-element mesh. These blocks are then assigned to different processors. This approach enables creation of the matrix in parallel. Since nodes in the matrix may be shared by elements belonging to different partitions, there will be some matrix blocks that are shared by the different processors. Once each processor creates its assigned matrix blocks, it will perform the factorization and update the shared blocks. Then the shared blocks will be factorized.

The shared blocks represent the *serial* portion of the factorization problem. Usually every problem has such a serial portion that must be executed by a single processor. This effect, characterized by the *Amdhal's law*, limits the number of processors that can be efficiently employed by a given problem. Fortunately, as the size of the problem increases, the size of this serial portion grows slower than that of the parallel portion. Thus, larger problems can use multiple processors more efficiently. For instance, when a 17000 node spherical mesh is distributed to two processors, the size of the common block is 5.54% of all nodes. For a 131000 node mesh, the common block only contains 2.79% of the nodes.

The parallel algorithm discussed above is implemented using the PVM library and tested on a local area network consisting of two Pentium II 300 Mhz Windows NT workstations; connected by a 100Mb/s fast ethernet network. A speed-up of 1.49 is obtained for a 31769 noded mesh. The memory requirement of 90.4 MB is shared among the processors almost evenly (49.9MB / 42.3 MB). Larger matrices can be solved by using additional computers in the cluster.

3.2. Boundary Element Method

BEM is based on integral equations which represent the fields in terms of basic solutions (for example, the unbounded case) and contribution of secondary sources at the interfaces. The surface integrals related to these secondary sources are approximated by dividing integration domains into a set of elements.

Forming a realistic representation of the head is important in numerical calculations. In order to represent the different conductivity interfaces shown in Fig. 4 the boundary element mesh can be constructed with shells representing conductivity interfaces. Fig. 8 shows a section of a spherical boundary element mesh of 3 layers representing brain, skull, scalp interfaces with quadratic type elements.

In order to solve the forward problem using boundary element method, the related differential equations are transformed into the integral form [47]. For any point defined at $\vec{r}$ in volume V, the potential Φ can be expressed as

$$\Phi(\vec{r}) = \frac{1}{4\pi\sigma}\int_{V'} \vec{J}_p(\vec{r}') \cdot \frac{\vec{R}}{R^3} dV' + \frac{1}{4\pi\sigma}\sum_k \int_{S_k} \Delta\sigma_k \Phi(\vec{r}') \frac{\vec{R}}{R^3} \cdot d\vec{S}'_k \tag{15}$$

while $\vec{B}$ can be obtained using the following integral equation [47],

$$\vec{B}(\vec{r}) = \frac{\mu_o}{4\pi}\int_{V'} \vec{J}_p(\vec{r}') \times \frac{\vec{R}}{R^3} dV' - \frac{\mu_o}{4\pi}\sum_k \int_{S_k} \Delta\sigma_k \Phi(\vec{r}') \frac{\vec{R}}{R^3} \times d\vec{S}'_k \tag{16}$$

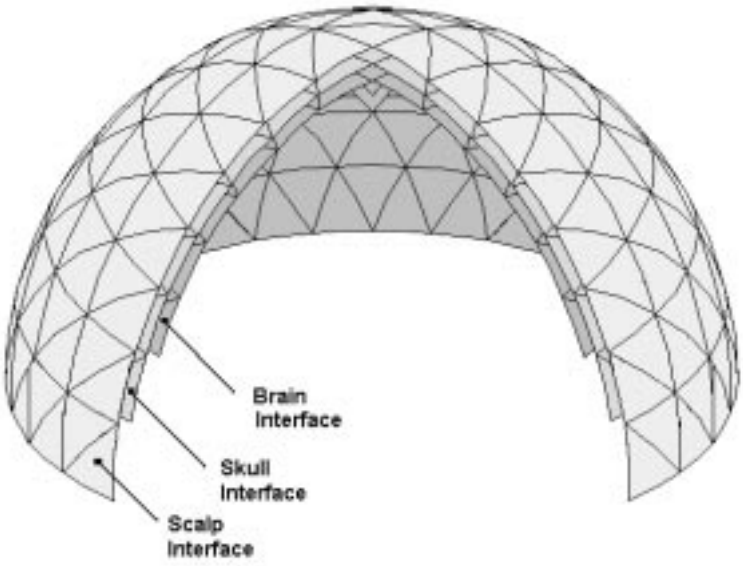

Figure 8. A section of a spherical boundary element mesh having 3 layers representing brain, skull, scalp interfaces. The mesh is composed of quadratic elements with 6 nodes as shown on the right.

In these formulations $\vec{R} = \vec{r} - \vec{r}'$ is the vector between the measurement and source points, V' represents the volume of the source region within the conductive body V, S_k is the surface of the k^{th} homogeneous conductive region, and $\Delta\sigma_k$ is the difference of conductivity across the boundary of the k^{th} conductivity region in the direction of $d\vec{S}_k$.

The first term in the above equation (volume integral) gives the potential distribution when the region is unbounded. The second term is the effect of secondary sources at the conductivity interfaces. In a simple multilayer head model, the scalp, skull, cerebrospinal fluid and brain are the major tissue types that produce conductivity interfaces [48]. In recent studies for magnetic measurements, the effects of outer layers are usually ignored and the head model is constructed as a homogeneous brain shaped volume [49].

To solve the above equations numerically, the surface S_k is discretized into N area elements. The surface integration in the above equation can then be obtained by summing up the integrals on these elements:

$$\int_{S_k} \Delta\sigma_k \Phi(\vec{r}') \frac{\vec{R}}{R^3} \cdot d\vec{S}' = \sum_{i=1}^{N} \int_{S_k^i} \Delta\sigma_k \Phi(\vec{r}') \frac{\vec{R}}{R^3} \cdot d\vec{S}_i{}' \tag{17}$$

where S_i represents the surface of the ith element. On each element, Φ is represented by a number of interpolation functions. The potentials produced at the nodes of a boundary element mesh can be obtained from the following matrix equation

$$\Phi = C\Phi + G \tag{18}$$

where Φ is a column vector of potentials and C is a deflated [50] square matrix (all eigenvalues less than 1) whose elements are determined by the geometry and electrical conductivities of the regions of the model.

Here G is the column vector of potentials when the source is in an infinite medium of unity conductivity. The potentials can be calculated as follows

$$\Phi = [I - C]^{-1} G \tag{19}$$

Once Φ is obtained the magnetic fields can be obtained by evaluating the integral expression given by equation 16.

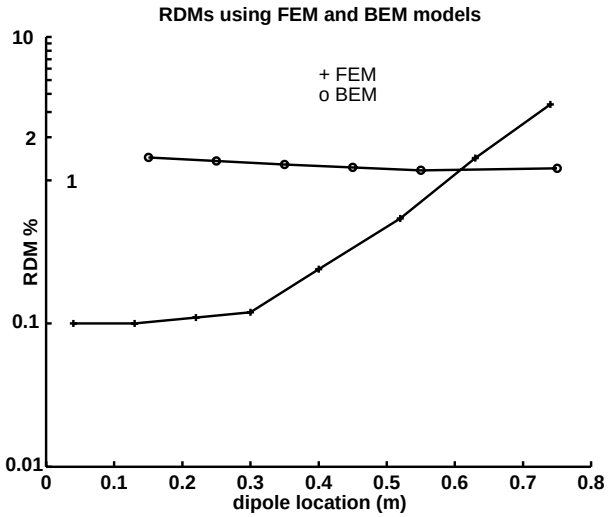

Figure 9. RDMs for the potential solutions using FEM and BEM models

3.3. Comparison of FEM and BEM

In order to understand the performance of the FEM and BEM, the corresponding numerical results are compared. The meshes used for each method has approximately the same number of *surface nodes* (1154 for FEM 1048 for BEM). For both methods isoparametric quadratic elements are used (20-noded hexahedral elements for FEM, 6-noded quadratic elements for BEM). The head model consists of three concentric spheres (radii 0.8, 0.9 and 1.0 m) with conductivities 0.2 S/m for inner sphere (brain) and outer sphere (scalp) and 0.005 S/m for the midle layer (skull). The results of each numerical method are compared to the analytical solutions using Relative Difference Measure (RDM). Figure gives the results of this comparison. It is observed that both FEM and BEM models yield RDMs around 1%. The relative superiority of BEM for shallow sources is due to inadequate source modeling used in the FEM. In order to represent a dipole at a certain depth, a number of volume elements are used. Since the size of the volume elements are larger near the sphere surface, especially the shallow dipole sources are not exactly modeled. It is concluded that this type of error can be decreased by modifying the mesh geometry or increasing the number of elements in the mesh.

The two numerical methods BEM and FEM have relative merits when solving for the potential on the scalp and the magnetic field just outside the head. BEM, as the name implies, only requires a mesh at the boundaries of each region, which generates solutions only at the boundaries. FEM on the other hand requires meshing of the full domain of interest, thereby yielding large number of elements and nodes but solutions are generated for the entire domain. Solutions of the potential and magnetic field can be calculated using BEM with fewer elements and equal accuracy levels compared to FEM solutions. However the coefficient matrix of BEM is not sparse. Computation cost for the BEM coefficient matrix is $O(N^2)$ where N is the

number of nodes in the mesh. Computing the FEM mesh is much easier, only $O(N)$ operations are needed. The resulting FEM coefficient matrix is sparse. It has a maximum of 81 non-zero elements on each row of the matrix. While factorizing the full BEM matrix is $O(N^3)$, the computational cost of factorizing a sparse matrix varies depending on the matrix structure and ordering of the matrix nodes [42].

When small size inhomogeneities and anisotropy are be taken into account, the FEM seems to be a more suitable technique. However, creating a realistic FEM mesh for the whole volume is a more difficult task than obtaining a realistic BEM mesh.

4. Conclusion and Discussion

Realistic models are the key elements in obtaining more accurate source distributions that represent the neural activity in the human brain. The purpose of this study was to introduce the problem of developing realistic head models in all aspects. Initially, the tissue classification problem was discussed. Since the classification of tissues in MR images via manual segmentation is tedious and time-consuming, the segmentation process needs to be automated. However, a satisfactory fully-automated MR image segmentation system has not been achieved yet. Among the proposed segmentation schemes, the deformable models seem to be the most promising ones, especially when the segmentation process is to be integrated with the mesh generation steps for the solution of the electro-magnetic source imaging problem.

Two numerical methods were introduced to solve the electric potential and magnetic field for arbitrary geometries and conductivity distributions. The numerical results obtained for single dipole sources at different depths show that it is possible to obtain solutions with RDMs less than 1%. The parallel implementation of the FEM was discussed to provide a means for solving large size problems using the computational equipment in a small size laboratory environment. The implemented parallelization algorithm provided a speed-up of 1.49 on two processors, for a 31769 noded mesh. The memory requirement was shared among the processors almost evenly (49.9MB / 42.3 MB).

By combining the resources of available computing facilities, it is possible to solve FEM problems that are too time consuming for a single workstation. As the performance of the workstations and local area networks increase as the workstation cluster becomes an attractive platform for high performance computing. However, to gain the maximum efficiency from parallel platforms the algorithms must be carefully selected, revised and tuned.

Note that all methods that are discussed in this paper are suitable also for finding electrical source distributions on the heart surface. For that purpose, the thorax geometry and electrical properties should be employed to develop a realistic torso model of the individual. The electrical and magnetic measurements can also be obtained from the torso surface and near the torso.

References

[1] M. E. Phelps, E.J. Hoffman, N. A. Mullani, and M. M. Ter-Pogossian. Application of Annihilation Coincidence Detection to Transaxial Reconstruction Tomography. *J. Nucl. Med.*, 16:210, 1975.

[2] Z. H. Cho, C. H. Oh, C. W. Mun, and Y. N. Kim, Some Results of High-Flow-Velocity NMR Imaging Using Selection Gradient. *Magn. Reson. Med.*, 3:857-2, 1986.

[3] D. G. Norris, J. M. S. Hutchison, Gated Cardiac Imaging Using Low-Field NMR. In *Phys. Med. Biolog.* 31(7):779-787, 1986.

[4] Y. S. Kim, C. W. Mun., K. J. Jung and Z. H. Cho, Further Improvement of High-Speed NMR Flow-Velocity Measurement Using a Differential Phase-Encoding Technique. *Magn. Reson. Med.*, 4:289, 1987.

[5] D. G. Nishimura, A. Macovski, and J. M. Pauly, Magnetic-Resonance Angiography, *IEEE Trans. Med. Imag.* MI-5, 1986.

[6] A. M. Dale, and M. I. Sereno, Improved Localization of Cortical Activity by combining EEG and MEG with MRI Cortical Surface Reconstruction: A Linear Approach. *Journal of Cognitive Neuroscience* 5:2, 1993.

[7] J. E. Knuutila, A. I. Ahonen, M. S. Hämäläinen, M. J. Kajola, P. P. Laine, O. V. Lounasmaa, L. T. Parkkonen, J. T. Simola and C. D. Tesche, A 122-channel whole-cortex SQUID system for measuring the brain's magnetic fields, *IEEE Transactions on Magnetics* 3315-3320 1993.

[8] A. I. Ahonen, M. S. Hämäläinen, M. J. Kajola, P. P. Laine, O. V. Lounasmaa, L. T. Parkkonen, J. T. Simola and C. D. Tesche, 122-Channel SQUID instrument for investigating the magnetic signals from the human brain, *Physica Scripta* T49:198-205, 1993.

[9] J. C. DeMunck, B. W. van Dijk, H. Spekreijse, Mathematical dipoles are adequate to describe realistic generators of human brain activity, *IEEE Trans. Biomed. Eng.*, 35:960, 1988.

[10] B. N. Cuffin. On the use of electric and magnetic data to determine sources in a volume conductor. *Ann. Biomed. Eng.,* ,6:173-193, 1978

[11] B. N. Cuffin, K. Yunokuchi, R. Maniewski, C. Purcell, G. R. Cosgrove,J. R. Ives, J. Kennedy, D. Schomer, MEG versus EEG localization test using implanted sources in the human brain. *Ann Neurol* 28:811-817,1990.

[12] D. L. Schomer, G. R. Cosgrove, H. W. Blume, J. R. Ives, B. N. Cuffin, D. Cohen Using dipole sources implanted in the human brain to compare MEG vs. EEG localization accuracy: The clinical significance, *Epilepsia* 31:623, 1990.

[13] B. N. Cuffin, D. Cohen, K. Yunokuchi, R. Maniewski, C. Purcell, G. R. Cosgrove, J. R Ives, J. Kennedy, D. Schomer, Tests of EEG localization accuracy using implanted sources in the human brain. *Ann Neurol* 29:132-138,1991.

[14] N. G. Gencer, S. J. Williamson, Differential characterization of Neural Sources with the Bimodal Truncated SVD Pseudo-inverse for EEG and MEG measurements, *IEEE Trans. Biomed. Eng.* 45(7):827-838

[15] A.K. Jain, Fundamentals of Digital Image Processing, Prentice-Hall, 1989.

[16] W.M. Wells et al., Adaptive segmentation of MRI data. *IEEE Transactions on Medical Imaging*, 15(4):429–442, August 1996.

[17] M.E. Brummer et al., Automatic Detection of Brain Contours in MRI Data Sets. *IEEE Transactions on Medical Imaging*, 12(2):153–166, June 1993.

[18] M.S. Atkins and B.T. Mackiewich, Fully Automatic Segmentation of the Brain in MRI, *IEEE Transactions on Medical Imaging*, 17(1):98–107, February 1998.

[19] J.C. Bezdek, L.O. Hall, and L.P. Clarke, Review of MR image segmentation techniques using pattern recognition, *Medical Physics*, 20(4):1033–1048, July/August 1993.

[20] L.O. Hall et al, A comparison of neural networks and fuzzy clustering techniques in segmenting magnetic resonance images of the brain, *IEEE Transactions on Neural Networks*, 3:672–683, 1992.

[21] L.D. Cohen and I. Cohen, Finite-Element Methods for Active Contour Models and Balloons for 2-D and 3-D Images, *IEEE Transactions on Pattern Analysis and Machine Intelligence*, 15(11):1131–1147, November 1993.

[22] S. Lobregt and M.A. Viergever, A Discrete Dynamic Contour Model, *IEEE Transactions on Medical Imaging*, 14(1):12–24, March 1995.

[23] R.P. Grzeszczuk and D.N. Levin, "Brownian Strings": Segmenting Images with Stochastically Deformable Contours, *IEEE Transactions on Pattern Analysis and Machine Intelligence*, 19(10):1100–1114, October 1997.

[24] C.A. Davatzikos and J.L. Prince, An Active Contour Model for Mapping the Cortex, *IEEE Transactions on Medical Imaging*, 14(1):65–80, March 1995.

[25] M. Kass, A. Witkin, and D. Terzopoulos, Snakes: Active contour models, *International Journal of Computer Vision*, 1:321–331, 1987.

[26] J.W. Snell et al, Model-based boundary estimation of complex objects using hierarchical active surface templates. *Pattern Recognition*, 28(10):1599–1609, 1995.

[27] H. Tek and B.B. Kimia, Volumetric segmentation of medical images by three-dimensional bubbles, *Computer Vision and Image Understanding*, 65(2):246–258, February 1997.

[28] A. Yezzi et al, A geometric snake model for segmentation of medical imagery, *IEEE Transactions on Medical Imaging*, 16(2):199–209, April 1997.

[29] D.J. Schlesinger et al, Segmentation of volumetric medical imagery using multiple geodesic-based active surfaces, In *Proceedings of SPIE Medical Imaging*, 1996.

[30] S. Sandor and R. Leahy, Surface-based labeling of cortical anatomy using a deformable atlas, *IEEE Transactions on Medical Imaging*, 16(1):41–54, February 1997.

[31] P. Thompson and A.W. Toga, A surface-based technique for warping three-dimensional images of the brain, *IEEE Transactions on Medical Imaging*, 15(4):402–417, August 1996.

[32] M. Thevenet, O. Bertrand, F. Perrin, T. Dumont, and J. Pernier, The finite element method for a realistic head model of electrical brain activities: Preliminary results, *Phys. Phsiol. Meas.,* 12, Supp. A:89-94, 1991.

[33] Y. Yan, P. L. Nunez, and R. T. Hart, A finite element model for the human head: Scalp potentials due to dipole sources, *Med. and Biol. Eng. and Comput.* , 29:475-481, 1991

[34] J. Le ve A. Gevins, Method to reduce blur distortion from EEG's using a realistic head model, *IEEE Trans. Biomed. Eng.*, BME-40: 517-528, 1992

[35] E. Hinton and D. R. J. Owen, *Finite Element Programming*, Academic Press, New York, 1983.

[36] P. Dasgupta, Z. M. Kedem, M. O. Rabin, Parallel Processing on Networks of Workstations: A Fault-Tolerant Approach, *15th Intl. Conf. on Distributed Computing Systems*, May 1995.

[37] T. Sterling, D. SAvarese, D. J. Becker, J. E. Dorband, U. A. Ranawake ve C. V. Packer, BEOWULF: A Parallel Workstation for Scientific Computation, *24th International Conference on Parallel Processing*, August 1995.

[38] A. Geist, A. Beguelin, J. Dongarra, W. Jiang, R. Manchek ve V. Sunderam, PVM: Parallel Virtual Machine - *A User's Guide and Tutorial for Networked Parallel*

[39] The MPI Home Page, available on the internet at: *http://www.mcs.anl.gov/mpi/index.html.*

[40] C. E. Acar A Parallel Processing Library for Personal Computers Connected to a Local Area Network, *MSc. Thesis*, Electrical and Electronics Engr. Dept., METU, September 1996.

[41] C. E. Acar, N. G. Gençer, Sonlu Elemanlar Sayısal Modelinin Çözümü için Kullanılan Yöntemlerin ve Sıralama Algoritmalarının Karşılaştırılması, *Elektrik-Elektronik Bilgisayar Mühendisliği 7. Ulusal Kongresi*, Eylül 1997.

[42] A. George, J. W. H. Liu, Computer Solution of Large Sparse Positive Definite Systems, Prentice Hall, 1981.

[43] I. Babuska, H.C. Elman, Some Aspects of parallel implementation of the finite-element method on message passing architectures, *Journal of Computational and Applied Mathematics*, 27, 1989.

[44] G. Karypis, V. Kumar, A High Performance Sparse Cholesky Factorization Algorithm For Scalable Parallel Computers, *Technical report 94-41, Dept. of Computer Science*, Univ. Minnesota, 1994.

[45] A. Gupta, G. Karypis, V. Kumar, Highly Scalable Parallel Algorithms for Sparse Matrix Factorization, *IEEE Trans. on Parallel and Distributed Systems*, Vol:8 No:5, Mayis 1997.

[46] G. Karypis, V. Kumar, METIS: Unstructured graph partitioning and sparse matrix ordering system, Technical Report, Department of Computer Science, University of Minnesota, 1995. Available on the WWW at URL *http://www.cs.umn.edu/ karypis/metis*

[47] D. B. Geselowitz. On bioelectric potentials in an inhomogeneous volume conductor. *Biophys. J.*, 7(1):1-11, 1967.

[48] S. Rush and D. A. Driscoll, EEG electrode senstivity:An application of reciprocity, *IEEE Trans. Biomed. Eng.* , BME-16:15-22, 1969.

[49] Matti S. Hämäläinen and Jukka Sarvas, Realistic Conductivity Model of the Human Head for Interpretation of Neuromagnetic Data *IEEE Trans. On Biomedical Engineering*, 36(2), 1989.

[50] M.S. Lynn and W.P. Timlake, The use of multiple deflations in the numerical solution of singular systems of equations with applications to potential theory *SIAM J. Numer. Anal.*, 5(2):303-322, 1968.